



Strain effects on the lattice thermal conductivity of monolayer CrOCl: A first-principles study

Ben-Yu Yu ^a, Yang Sun ^a, Xinrui Cao ^{a,b}, Zi-Zhong Zhu ^{a,b}, Shunqing Wu ^a, Tie-Yu Lü ^{a,*}

^a Department of Physics, OSED, Key Laboratory of Low Dimensional Condensed Matter Physics (Department of Education of Fujian Province), Xiamen University, Xiamen 361005, China

^b Fujian Provincial Key Laboratory of Theoretical and Computational Chemistry, Xiamen University, Xiamen 361005, China

ARTICLE INFO

Keywords:

Monolayer CrOCl
Thermal transport
Boltzmann transport equation
First-principle
Strain effect

ABSTRACT

Monolayer CrOCl is an intrinsically ferromagnetic two-dimensional semiconductor material with potential applications in nano-spintronic devices, which call for fundamental studies of phonon transport. Here, we investigate the lattice thermal conductivity of monolayer CrOCl under uniaxial strain using first-principles calculations to solve the phonon Boltzmann transport equation. At 300 K, the lattice thermal conductivities of monolayer CrOCl are $47.00 \text{ Wm}^{-1}\text{K}^{-1}$ (x direction) and $123.97 \text{ Wm}^{-1}\text{K}^{-1}$ (y direction), exhibiting significant anisotropy. Applying uniaxial strains of $-2\%-2\%$ to monolayer CrOCl in the x and y axes, we discovered that both compressive and tensile strains reduced the thermal conductivity of monolayer CrOCl. By analyzing the responses of heat capacity, phonon group velocity, and phonon lifetime to strain, we determined that the rapid decrease in phonon lifetime under strain is the primary cause of the decrease in thermal conductivity.

1. Introduction

The successful exfoliation of graphene [1] has incited substantial interest among scientists in exploring two-dimensional (2D) materials. The research into their application in electronic devices is a crucial focus, with a vision to design next-generation, highly efficient, low-power electronic devices using their quantum effects [2–5]. As these devices downsize, several challenges emerge, including severe heat accumulation under saturation current operating conditions, which can lead to increased device temperature, performance degradation, and even device burn out [6–10].

Therefore, rapidly conducting away waste heat is a vital consideration in electronic device design. While graphene possesses high thermal conductivity ($2500\text{--}5000 \text{ Wm}^{-1}\text{K}^{-1}$ for suspended graphene and $600 \text{ Wm}^{-1}\text{K}^{-1}$ for substrate-based graphene) [11–13], its semi-metallic nature imposes limitations on its utility in electronic devices. Hexagonal boron nitride (h-BN), with its large band gap and high thermal conductivity ($751 \text{ Wm}^{-1}\text{K}^{-1}$) [14], is an ideal candidate for 2D semiconductor devices. Despite the lower thermal conductivity of anisotropic 2D materials such as phosphorene compared to h-BN, the added modulation dimension allows these materials to have unique thermal management benefits. Ong et al. demonstrated that in

anisotropic 2D materials, heat is typically dissipated quickly along the high thermal conductivity direction without accumulating in the channels [15]. Additionally, the characteristics of material anisotropy can be utilized to modulate thermal transport effectively, promoting rapid heat conduction along the high thermal conductivity direction while providing thermal insulation in the low thermal conductivity direction [16–18].

Two-dimensional CrOCl has garnered researcher interest due to its potential applications in self-gating electronic devices [19–21]. The surface anisotropy and magnetic properties of CrOCl, combined with its layered structure, offer novel physical properties when integrated with other 2D materials to form heterojunctions. For instance, anomalous quantum Hall effects occur in monolayer graphene/CrOCl [22]. Furthermore, bilayer graphene/CrOCl hetero-system can induce an insulating state with over $1\text{-G}\Omega$ resistance across a broad range of gate voltages, which can be transitioned to a metallic state using a planar electric field, heating, or gate control [23]. Additionally, the anisotropy and large band gap of CrOCl, in both its bulk and 2D forms, offer potential utility in thermal management for electronic devices.

The operating temperature of electronic devices can significantly affect their performance, and the thermal transport properties of 2D-CrOCl remain understudied. To our knowledge, only Zheng et al. have

* Corresponding author.

E-mail address: ty@xmu.edu.cn (T.-Y. Lü).

measured the thermal conductivity of a few layers of CrOCl using micro-Raman thermometry [24]. The thermal conductivity of a single layer of CrOCl was not measured due to experimental constraints. Moreover, the lattice mismatch between different materials within the heterojunction can induce strain in the material, altering its physical properties. However, reports on the variation of 2D-CrOCl thermal conductivity with strain are absent.

In this paper, we examine the thermal conductivity of monolayer CrOCl in its equilibrium state using first-principles calculations based on Density Functional Theory (DFT), combined with the Boltzmann Transport Equation (BTE) method. We also discuss the relationship between its thermal conductivity and uniaxial strain. Our study lays a theoretical groundwork for efficient thermal management in future nanoscale electronic devices using 2D-CrOCl.

2. Method and calculation details

We conducted first-principles calculations based on density functional theory (DFT) using the VASP software program [25]. The Perdew-Burke-Ernzerhof (PBE) [26] generalized gradient approximation (GGA) was selected as the exchange-correlation functional. To ensure the absence of interlayer interactions, vacuum layers larger than 10 Å were employed. Structural optimization was performed using a plane wave basis set with a kinetic energy cutoff of 520 eV, and a $13 \times 15 \times 1$ grid was used for Monkhorst-Pack k-point sampling. The energy convergence criterion was set to 10^{-5} eV, while the force convergence criterion was set to 10^{-3} eV/Å. To accurately account for the strong correlation effects of electrons, a correction was applied by introducing U values of 7 eV, in accordance with prior research [19]. In addition, the van der Waals (vdW) interaction cannot be ignored when it comes to the physical properties of two-dimensional materials. Therefore, we take into account the vdW correction in our calculations, employing the D3-Grimme method [27].

In our study, we investigated the effects of uniaxial strain on the monolayer CrOCl structure. To apply the strain, we subjected the material to uniaxial strains in the x and y directions. The strains used were -2% , -1% , 1% and 2% . To quantify the applied strain, we defined the strain values as ε_x and ε_y . Here, ε_x (ε_y) represents the strain in the x (y) direction. These values were calculated using the following formula:

$$\varepsilon_x = (a - a_0) / a_0$$

$$\varepsilon_y = (b - b_0) / b_0$$

In these formulas, a and b are the lattice constants along the x and y directions for the strained structure, respectively. a_0 and b_0 are the lattice constants along the x and y directions for the fully relaxed structure. The positive strain values of ε_x (ε_y) indicate tensile strain, while negative strain values indicate compressive strain.

To ensure convergence and uniformity in the phonon dispersion calculations, we constructed a $5 \times 5 \times 1$ supercell containing 150 atoms for each structure. We used density functional perturbation theory (DFPT) in a linear response framework as implemented in the VASP code to obtain the second-order interatomic harmonic force constants (IFCs). PHONOPY [28,29] was employed to calculate the phonon dispersion relations for the monolayer CrOCl.

To calculate the lattice thermal conductivity, we needed both the second-order harmonic and the third-order anharmonic force constants (IFCs). We obtained the second-order IFCs as described above. We used a $4 \times 4 \times 1$ supercell to obtain the third-order anharmonic IFCs with a cutoff distance of 0.514 nm for the twelfth nearest neighbor interaction. To account for the long-range electrostatic interactions, we also calculated the DFPT-based dielectric tensor and the Born effective charge. We chose the effective thickness of a single layer of CrOCl to be 8.956 Å, which is the sum of the layer thickness and the van der Waals radii of the Cl atoms on the upper and lower surfaces. This thickness is required for the thermal conductivity calculation of a two-dimensional material. To

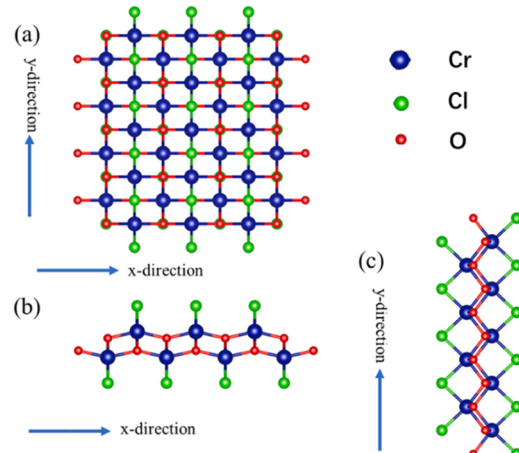


Fig. 1. Crystal structure of monolayer CrOCl.

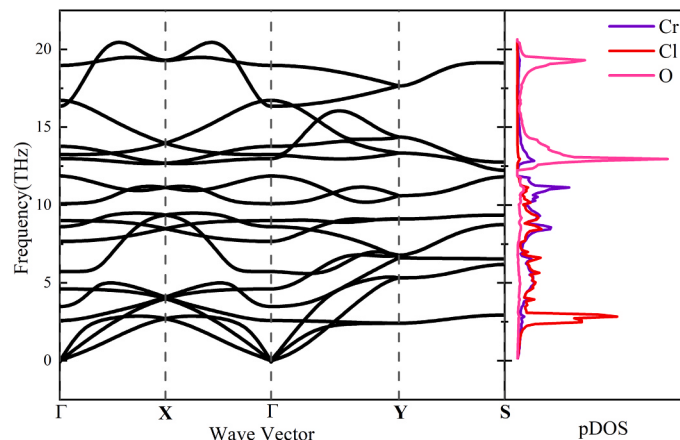


Fig. 2. Phonon dispersion relations and partial density of states of monolayer CrOCl along the high symmetry points.

obtain the intrinsic lattice thermal conductivity, we utilized the ShengBTE package [30]. This powerful tool enabled us to solve the phonon Boltzmann transport equation (BTE), specifically considering the phonon-phonon scattering process exclusively. According to the theory of phonon BTE, the lattice thermal conductivity (κ) at a specific temperature can be calculated by summing the contributions from all phonon modes and frequencies. For a specific direction, the calculation formula for lattice thermal conductivity is represented by Eq. 1:

$$\kappa_{\alpha} = \sum_{\lambda} c_{ph,\lambda} v_{\alpha,\lambda}^2 \tau_{\lambda} \quad (1)$$

where α represents the directional dependence of thermal conductivity in the specific direction, while $c_{ph,\lambda}$ represents the volumetric specific heat of the phonon mode λ which is defined by the wave vector q and phonon branch s . Furthermore, $v_{\alpha,\lambda}$ denotes the group velocity of the mode λ in direction α , and τ_{λ} represents the lifetime of the phonon mode λ .

3. Results and Discussion

3.1. Crystal structures and Phonon dispersion relation

The monolayer CrOCl has an orthorhombic structure. Fig. 1 shows the schematic diagram of the structure of monolayer CrOCl. The optimized lattice constants are 3.956 Å and 3.268 Å along the x and y directions, respectively, which agree well with the simulation results of

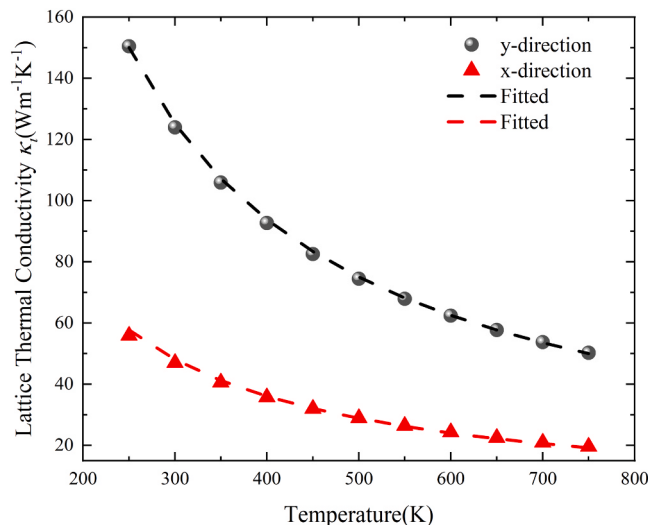


Fig. 3. Calculated lattice thermal conductivity of monolayer CrOCl along the x and y directions as a function of temperature ranging from 250 K to 750 K.

Miao et al. [19].

The phonon dispersion relation of monolayer CrOCl is shown in Fig. 2. Similar to other 2D materials including graphene [31], silicene [32] and phosphorene [33], monolayer CrOCl exhibits flexural phonon branches (which represent phonon vibration modes in the z direction, namely ZA phonons) in proximity to the Γ point, a characteristic commonly observed in 2D materials [31]. The group velocities of acoustic phonons along the Γ -X and Γ -Y directions, as shown in Fig. 2, are different, with the velocity along the Γ -X direction being smaller. The lattice asymmetry is responsible for this, and phosphorene exhibits similar behavior [33]. The highest frequency of normal phonon vibration mode (Debye frequency) is $\nu_m = 5.32$ THz, from which we can calculate the Debye temperature (θ_D) as: $\theta_D = h\nu_m/k_B = 255.25$ K, where h is Planck's constant and k_B is Boltzmann's constant. Fig. 2 also demonstrates the phonon partial density of states for monolayer CrOCl. It is evident that the acoustic branch at lower frequencies and the optical branch at intermediate frequencies primarily originate from the vibrations of the heavier atoms Cr and Cl. Meanwhile, the optical branch at higher frequencies primarily stems from the vibrations of the lighter atom O. This occurrence can be attributed to the tendency of lighter atoms to vibrate at faster rates compared to their heavier counterparts.

Fig. 2 shows that the main phonon frequency of Cr is higher than that of Cl, which defies the general trend that atomic mass correlates negatively with phonon frequency. We believe that this is caused by the following reasons. Among Cr, O, and Cl atoms, the Cr atom has the largest mass, and its main phonon frequency tends to be lower. Simultaneously, in a monolayer CrOCl structure, one Cr atom is surrounded by four O atoms and two Cl atoms. O atoms have a smaller mass, hence their phonon frequencies are higher, which prompts the Cr atom to vibrate at a higher frequency. These two opposing trends create a competitive relationship. Furthermore, Cl atoms form bonds only with Cr atoms and are located on the surface of the two-dimensional material. Eventually, this leads to a higher phonon frequency of Cr compared to Cl. Additionally, a comparative analysis of the phonon spectrum of IrOCl [34] can further confirm our speculation. In a monolayer IrOCl structure (where Ir atom replaces Cr atom and have a larger atomic mass than Cr), the main phonon frequency of Ir exhibits a significant decrease relative to the main phonon frequency of Cr. This serves as additional evidence for our explanation.

3.2. Intrinsic lattice thermal conductivity

The temperature-dependent behavior of lattice thermal conductivity

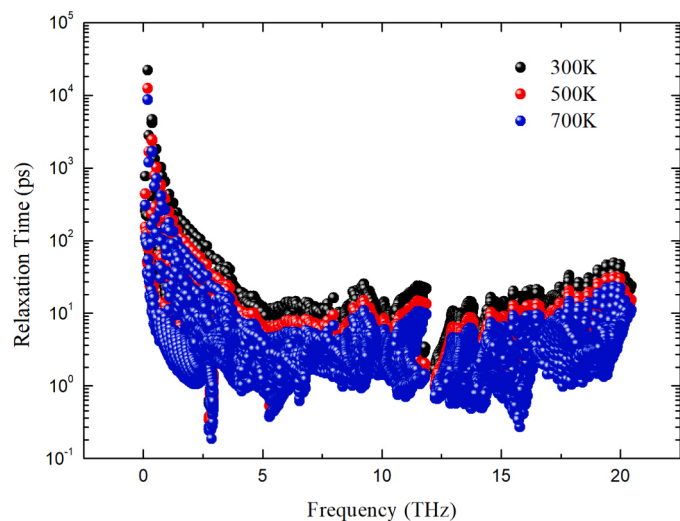


Fig. 4. Relaxation time of phonons as a function of phonon frequency at 300 K (black), 500 K (red) and 700 K (blue).

along the x and y axes is illustrated in Fig. 3. The thermal conductivity along the y direction is significantly greater than the x direction in monolayer CrOCl, showing an anisotropic lattice thermal conductivity similar to 2D materials like phosphorene [33], monolayer $\text{Ir}_2\text{Cl}_2\text{O}_2$ [34], and monolayer SnSe [35].

At 300 K, the lattice thermal conductivity of monolayer CrOCl is $47.00 \text{ W}\cdot\text{m}^{-1}\cdot\text{K}^{-1}$ in the x direction and $123.97 \text{ W}\cdot\text{m}^{-1}\cdot\text{K}^{-1}$ in the y direction. The experimental data [24] can be linearly fitted, yielding thermal conductivities of $114 \text{ W}\cdot\text{m}^{-1}\cdot\text{K}^{-1}$ and $319 \text{ W}\cdot\text{m}^{-1}\cdot\text{K}^{-1}$ for monolayer CrOCl in the x direction and y direction, respectively. Although the numerical simulation results are smaller than the experimental values, they exhibit good agreement in terms of anisotropy. The anisotropy ratios derived from numerical simulation and experimental measurement are 2.64 and 2.80, respectively.

The impact of long-range electrostatic interactions arising from the dielectric constant and Born effective charge on the lattice thermal conductivity was also investigated. The results reveal that neglecting long-range electrostatic interactions only leads to a marginal difference of approximately 2% in the calculated thermal conductivity.

In Fig. 3, we employed an inverse function to fit the relationship between the thermal conductivity and temperature along the x and y directions, which is illustrated by the dashed lines. Clearly, within the range of temperatures investigated, there exists an inverse relationship between the thermal conductivities of single-layer CrOCl and temperature, i.e. $\kappa \sim 1/T$. The main underlying cause for this phenomenon is that the number of excited phonons tends to be roughly proportional to the temperature, resulting in an inverse relationship between the mean free path and the phonon concentration. Consequently, the mean free path is inversely proportional to the temperature, ultimately leading to an inverse correlation between thermal conductivity and temperature. To further clarify this point, we conducted calculations of phonon relaxation times, or phonon lifetimes, at various temperatures and represented them against frequency for 300 K, 500 K, and 700 K in Fig. 4. It is evident that the phonon relaxation times for distinct phonon modes decrease to varying degrees as temperature increases. This indicates that higher temperatures substantially reduce phonon lifetimes, diminish the mean free path of phonons, and consequently weaken their thermal transport capacity. As a result, there is a consistent decrease in thermal conductivity with increasing temperature.

In comparison to the thermal conductivity of graphene ($3000\text{--}5000 \text{ W}\cdot\text{m}^{-1}\cdot\text{K}^{-1}$) [6], the thermal conductivity of single-layer CrOCl is lower by one to two orders of magnitude. In order to comprehend the underlying mechanism, we conducted an analysis of the

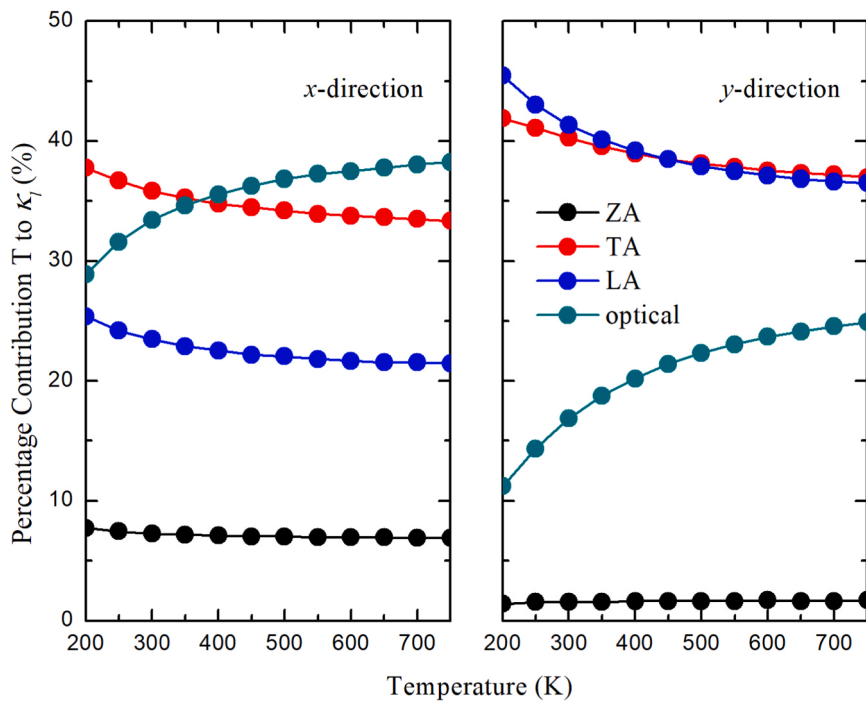


Fig. 5. Percentage contribution of different phonon branches of monolayer CrOCl to the lattice thermal conductivity as a function of temperature ranging from 200 K to 750 K.

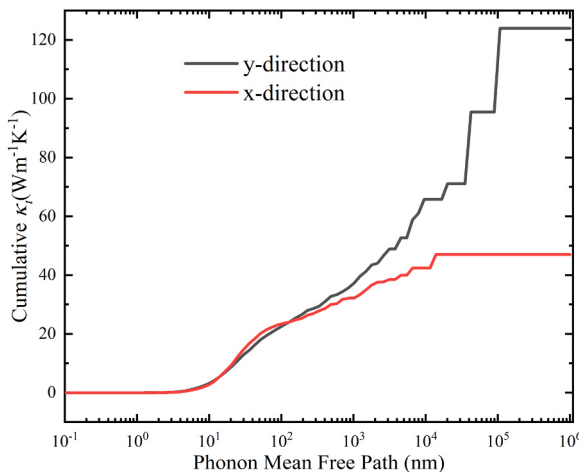


Fig. 6. Cumulative lattice thermal conductivity of monolayer CrOCl along x (red) and y (black) directions as a function of the phonon MFP at 300 K.

contributions from various phonon branches to the thermal conductivity of monolayer CrOCl in both the x and y directions. This analysis is depicted in Fig. 5. It is evident that the ZA phonon modes contribute less than 8% and 2% to the thermal conductivity in the x and y directions, respectively, at room temperature. While, the contribution of ZA phonons to the thermal conductivity of graphene is up to 75% [36]. Therefore, we suggest that the relatively low thermal conductivity of monolayer CrOCl may have the similar reason as that of phosphorene [33] and silicene [32]. The structure of monolayer CrOCl breaks the symmetric phonon-phonon scattering rule [37], resulting in a large scattering rate of the out-of-plane ZA phonon modes and hence a small contribution to the thermal conductivity. We also note that the acoustic phonon branch plays a dominant role in the phonon thermal transport process, contributing most of the lattice thermal conductivity. In Fig. 5, we observe that the optical branch of monolayer CrOCl contributes

significantly more to thermal conduction compared to phosphorene. As a result, monolayer CrOCl exhibits a higher thermal conductivity than phosphorene [33]. As the temperature increases, the contribution of the optical phonon branch increases while that of the acoustic phonon branch decreases. This is likely because the elevated temperature stimulates higher frequency optical phonon modes, allowing more optical phonons to engage in thermal transport, thereby augmenting their contribution to the lattice thermal conductivity. Specifically, when the temperature surpasses 360 K, the contribution of the optical branch along the x axis to thermal conduction even exceeds that of the TA branch.

Fig. 6 illustrates the correlation between the cumulative lattice thermal conductivity and the phonon mean free path (MFP) in both the x and y directions at 300 K. It is evident that the cumulative lattice thermal conductivity increases with the MFP until it reaches a plateau. This observation highlights the significant influence of the size effect on the material's thermal transport and its pivotal role in phonon thermal conduction. Exploiting this effect can effectively regulate the material's thermal conductivity. One relevant quantity associated with the size effect is the characteristic size, which is defined as the ratio of the thermal conductivity to the thermal conductivity per unit MFP in the small grain limit [38]. The formula is as follows:

$$\Delta l = \frac{\kappa_l}{\tilde{\kappa}_{SG}} \quad (2)$$

where κ_l is the lattice thermal conductivity and $\tilde{\kappa}_{SG}$ is the thermal conductivity per unit MFP in the small grain limit. The characteristic size serves as an approximate estimation of the scale at which phonon scattering caused by size effects surpasses anharmonic phonon scattering. This is of significance in the realm of thermal transport design utilizing nanostructures, as when the size of the nanostructure falls below the characteristic size, it becomes possible to effectively manipulate the thermal conductivity of the material through nanostructures. In the case of monolayer CrOCl, characteristic sizes of 65 nm and 197 nm were obtained in the x and y directions, respectively.

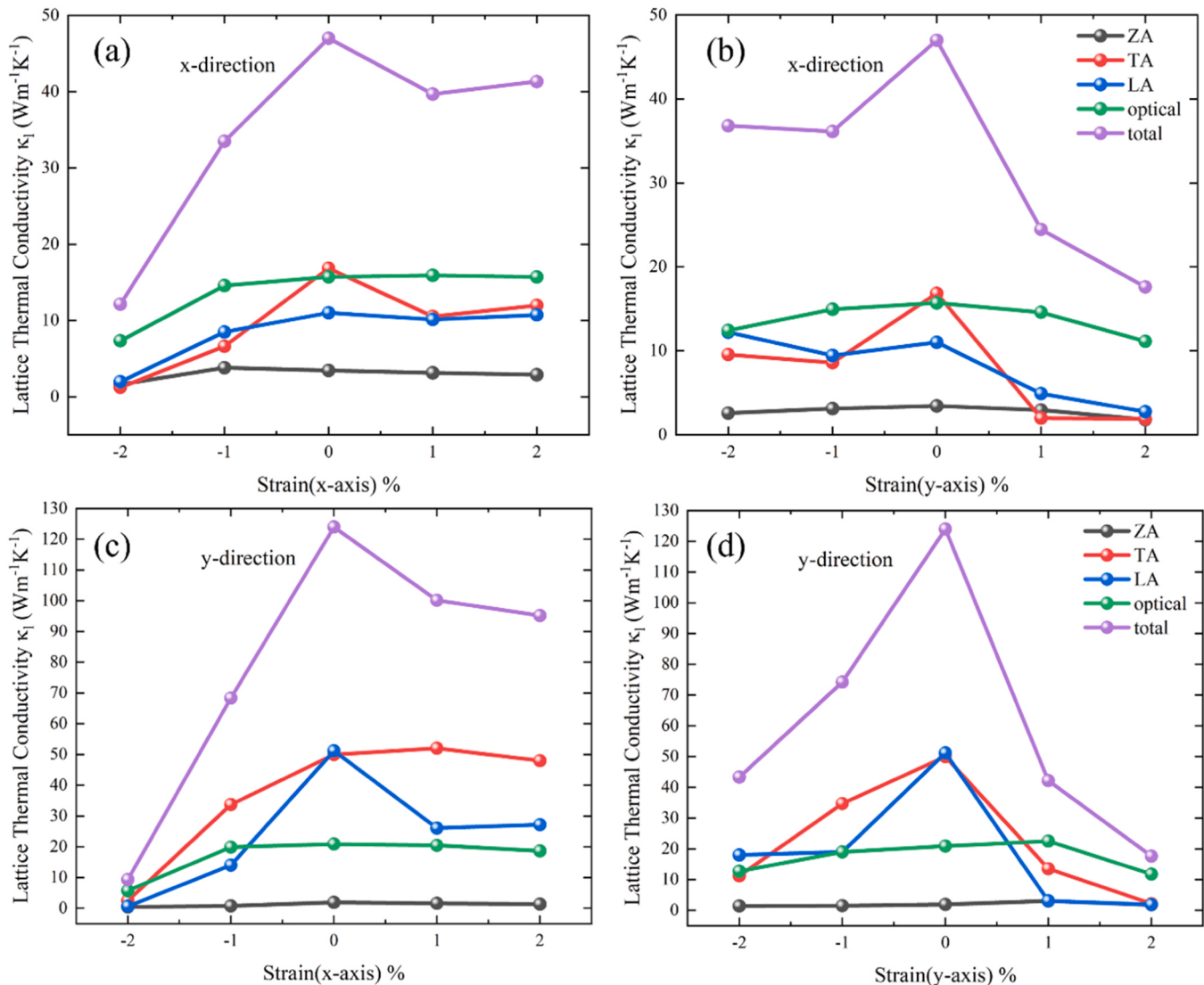


Fig. 7. Lattice thermal conductivity of monolayer CrOCl along x direction with x axis strain (a); x direction with y axis strain (b); y direction with x axis strain (c) and y direction with y axis strain (d), respectively, at 300 K.

3.3. Effects of strain on the lattice thermal conductivity

When incorporating 2D materials into nanodevices, they inevitably undergo deformation as a result of assembly constraints. Furthermore, when vertically stacking or laterally connecting different types of 2D crystals to create heterostructures, it is common for the 2D materials to experience strain due to lattice mismatch. On the other hand, utilizing strain as a means of manipulating the properties of 2D materials, including thermal transport properties, is a remarkably effective approach in the field of materials engineering [39]. In this study, we investigated the effect of uniaxial strain on the thermal conductivity of monolayer CrOCl along the x and y directions. Strains ranging from $-2\text{--}2\%$ were applied, with negative strains representing compressive strain and positive strains representing tensile strain.

The thermal conductivity values of monolayer CrOCl at 300 K under different strains are shown in Fig. 7. We note that the peak thermal conductivity occurs in the absence of strain, and both tensile and compressive strains caused a decrease in the thermal conductivity of monolayer CrOCl. This trend is consistent with the variations in thermal conductivity of graphene reported by X. Li *et al.* under different strains [40]. The phenomenon of fluctuating thermal conductivity with strain has also been observed in numerical simulations of other 2D materials,

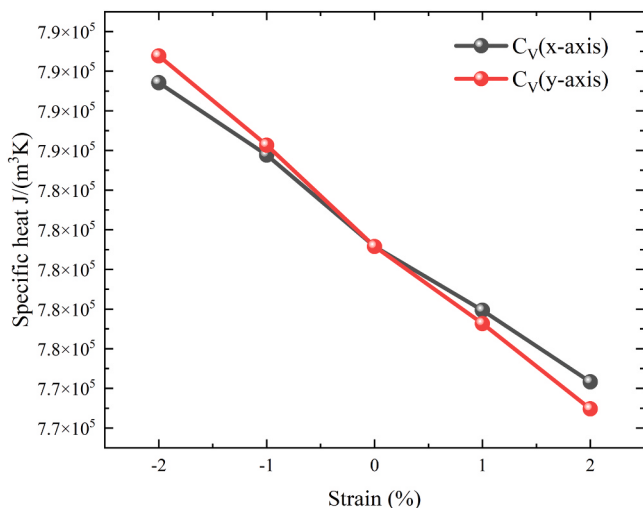


Fig. 8. Specific heat - uniaxial strain relationship at 300 K.

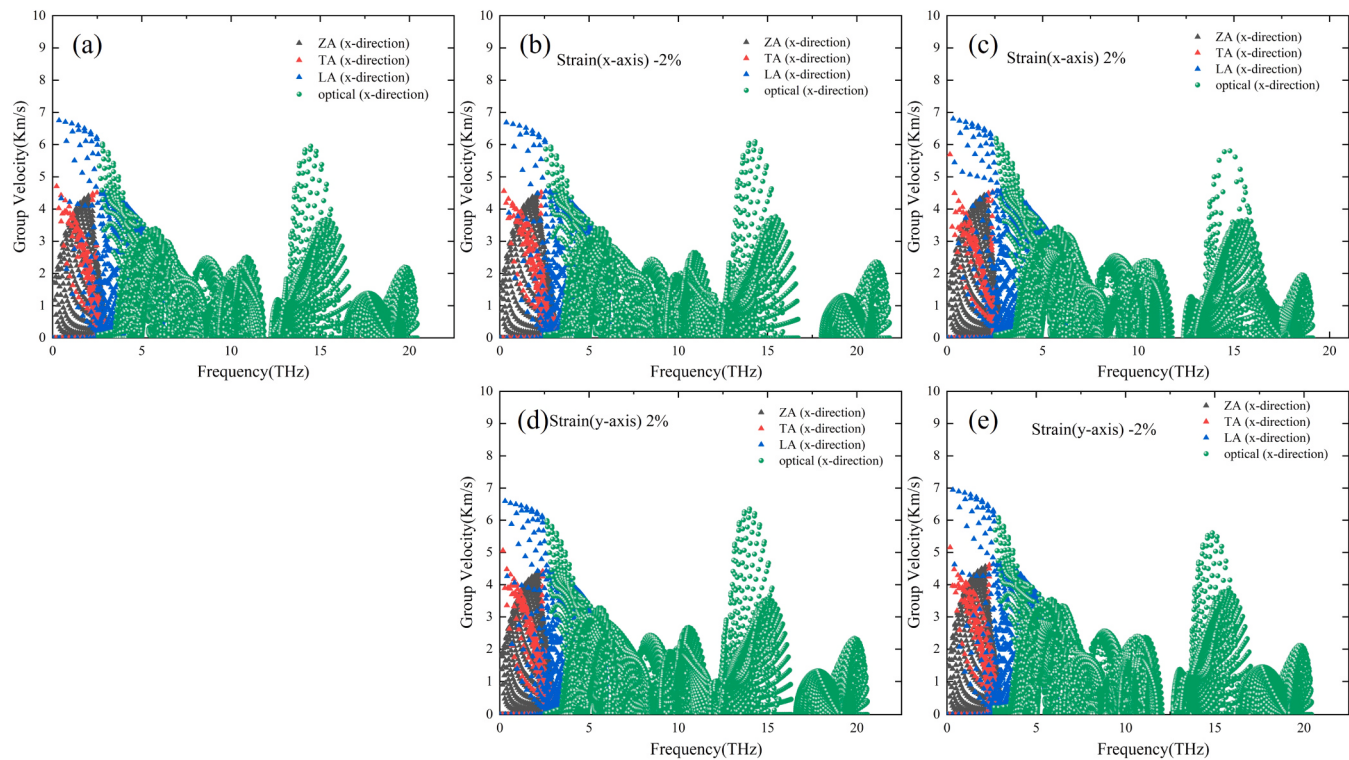


Fig. 9. Group Velocities along x direction of phonon branches with unstrained, 2% compressive and 2% tensile strains applied along the x axis and y axis, respectively, at 300 K.

such as silicene [41], penta-SiC₂ [42], and penta-NiN₂ [43]. Fig. 7 demonstrates that uniaxial compressive strain in the x axis direction has a greater impact on thermal conductivity compared to the y axis direction. Conversely, when subjected to tensile strain, the influence of uniaxial tensile strain in the y axis on thermal conductivity is greater than that in the x axis. Notably, in Fig. 7, we observe an intriguing phenomenon: the thermal conductivity along the x direction and y direction tends to be equal when applying either a 2% uniaxial compressive strain in the x axis or a 2% uniaxial tensile strain in the y axis to CrOCl. Further analysis reveals that the contributions of the ZA and optical branches to strain response are relatively small under uniaxial strain. The changes in thermal conductivity primarily arise from the responses of the LA and TA branches to strain.

According to Eq. 1, the varying relationship between thermal conductivity and strain in different 2D materials can be attributed to the distinct dependence of strain on heat capacity, group velocity, and phonon lifetime. These factors are influenced by the crystal structures of 2D sheets, following the principles of simple kinetic theory [39].

The specific heat capacity of unstrained monolayer CrOCl is 7.81×10^5 J/(m³·K) at 300 K. The influence of uniaxial strain on specific heat capacity at 300 K is illustrated in Fig. 8. As the strain varies from -2–2%, the specific heat capacity shows a consistent decreasing trend. The rate of change in specific heat capacity is slightly smaller for the x axis compared to the y axis. The trend of heat capacity change is significantly different from that of thermal conductivity change. Within the range of strain investigated in this study, the variation in specific heat capacity is found to be less than 1%. Hence, the impact of specific heat capacity on thermal conductivity is negligible, aligning with the outcomes reported by Xie et al. [41].

Fig. 9 shows the group velocities of phonons along the x direction for different uniaxial strains (-2%, 0, 2%). The results show that the group velocities of phonons are relatively insensitive to strain within the range of -2–2%. In particular, the group velocities of the ZA, TA, and LA acoustic branches are difficult to discern by eye. The change in group

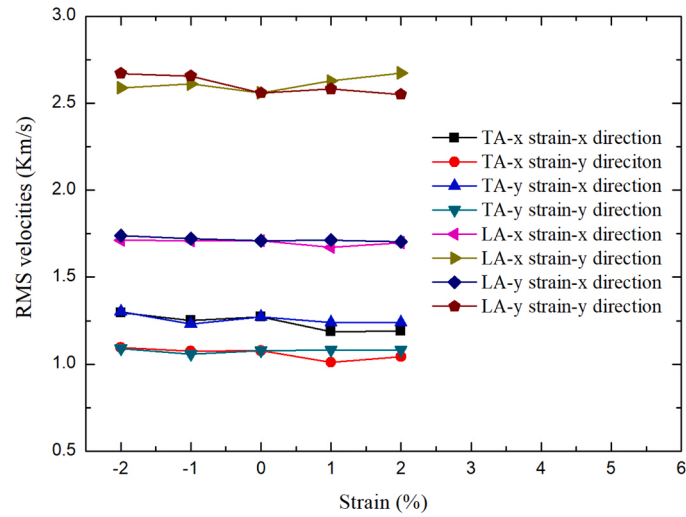


Fig. 10. Relationship between the root-mean-square (RMS) of the phonon group velocities for TA and LA modes and uniaxial strain.

velocities along the y direction is similar to that along the x direction and is also not significant. To quantify the effect of strain on the group velocity, we calculated the root mean square velocity. As shown in Fig. 10, the root mean square velocity of the LA phonon along the y direction increases with increasing x axis strain, while the root mean square velocities of the other TA and LA phonons decrease. The change in root mean square velocity for the TA and LA phonons is small (less than 1.7%). This small change in the root mean square velocity cannot explain the significant decrease in thermal conductivity observed under strain.

To further investigate the impact of uniaxial strain on thermal conductivity, we compare the lifetimes of phonons under strained and

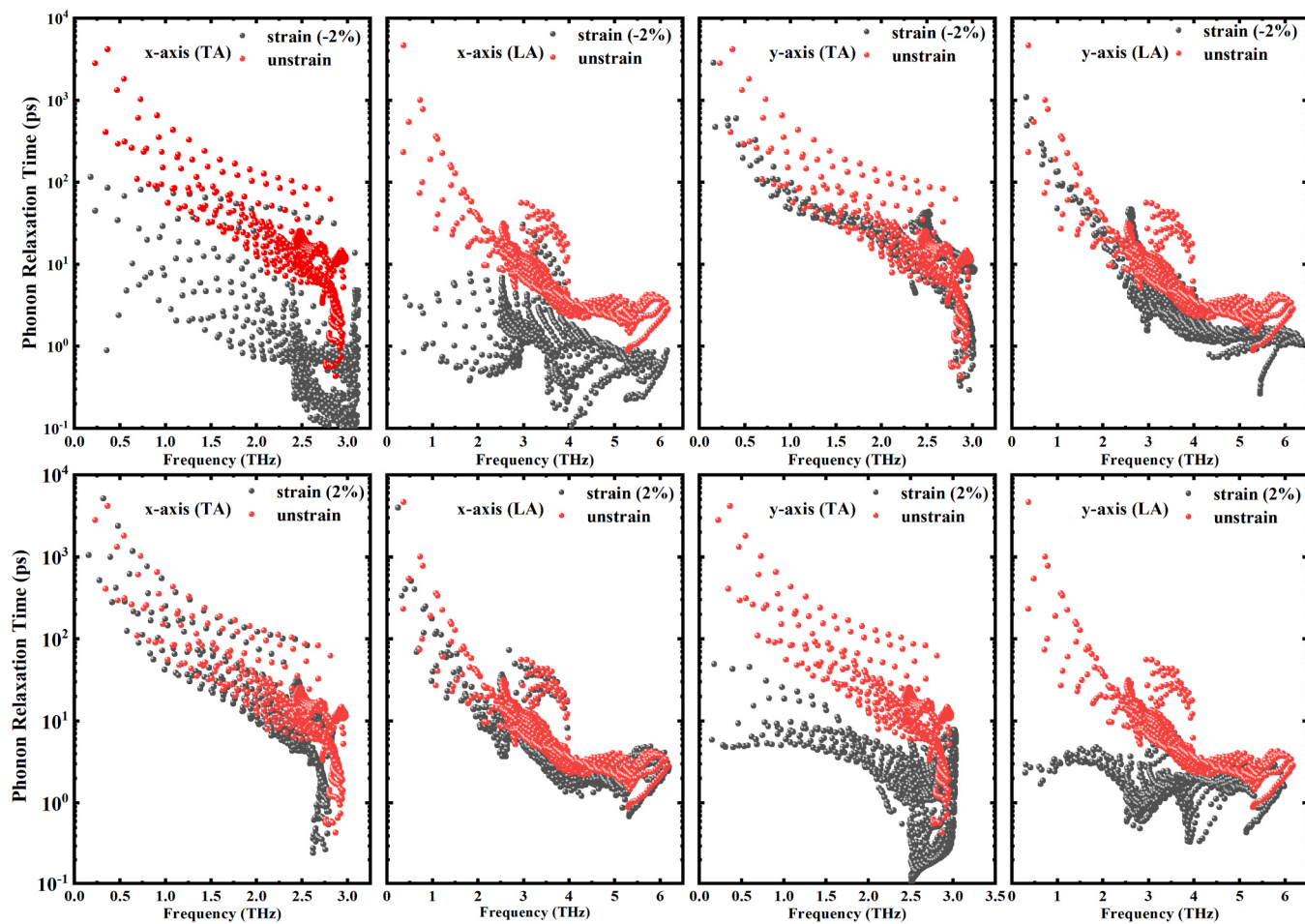


Fig. 11. Variations in the lifetimes of TA and LA phonons under both 2% compressive and 2% tensile strains applied along the x axis and y axis, respectively, at 300 K.

unstrained conditions, as depicted in Fig. 11. The figure specifically presents the lifetimes of TA and LA phonons under three different levels of uniaxial strain: -2%, 0%, and 2%. This selection is motivated by the fact that the changes in thermal conductivity of monolayer CrOCl under uniaxial strain primarily stem from variations in TA and LA phonons. Irrespective of whether the strain is compressive or tensile, both TA and LA phonons exhibit a general decrease in lifetime. Notably, a significant decrease in phonon lifetime, even by an order of magnitude, is observed for a 2% compressive strain along the x axis or a 2% tensile strain along the y axis. This trend is consistent with the observations in Fig. 7. These results underscore the crucial role of phonon lifetimes in determining thermal conductivity under uniaxial strain.

4. Conclusions

In summary, we used first-principles methods based on density functional theory to investigate the intrinsic thermal conductivity of monolayer CrOCl. When the temperature is higher than the Debye temperature ($\theta_D=255.25$ K), the calculated thermal conductivity is in perfect agreement with the inverse relationship with temperature. Due to the crystal symmetry, the thermal conductivity of CrOCl is not isotropic, which is similar to phosphorene. At 300 K, our calculations show that the thermal conductivities of CrOCl along the x and y directions are $47.00 \text{ W m}^{-1} \text{ K}^{-1}$ and $123.97 \text{ W m}^{-1} \text{ K}^{-1}$, respectively. The anisotropy ratio is in good agreement with the experimental results. In addition, we also calculated the representative phonon mean free paths along the x and y directions. When uniaxial strains of -2–2% were applied to monolayer CrOCl along the x and y axes, both compressive

and tensile strains would lead to a decrease in the thermal conductivity of monolayer CrOCl. By analyzing the responses of heat capacity, phonon group velocity, and phonon lifetime to strain, we found that the main reason for the decrease in thermal conductivity is that the phonon lifetime decreases rapidly under strain.

CRediT authorship contribution statement

Ben-Yu Yu (First Author): Software, Investigation, Data Curation, Formal Analysis, Visualization, Writing - Original Draft. **Yang Sun:** Formal Analysis, Supervision, Writing - Review & Editing. **Xinrui Cao:** Formal Analysis, Supervision, Writing - Review & Editing. **Zi-Zhong Zhu:** Conceptualization, Supervision. **Shunqing Wu:** Conceptualization, Supervision, Writing - Review & Editing. **Tie-Yu Lü (Corresponding Author):** Conceptualization, Methodology, Resources, Supervision, Writing - Review & Editing.

Declaration of Competing Interest

The authors declare that they have no known competing financial interests or personal relationships that could have appeared to influence the work reported in this paper.

Data Availability

Data will be made available on request.

References

- [1] K.S. Novoselov, A.K. Geim, S.V. Morozov, D.-e Jiang, Y. Zhang, S.V. Dubonos, I. V. Grigorieva, A.A. Firsov, Electric field effect in atomically thin carbon films, *Science* 306 (5696) (2004) 666–669.
- [2] A. Pospischil, M. Humer, M.M. Furchi, D. Bachmann, R. Guider, T. Fromherz, T. Mueller, CMOS-compatible graphene photodetector covering all optical communication bands, *Nat. Photonics* 7 (11) (2013) 892–896.
- [3] J. Li, X. Yang, Y. Liu, B. Huang, R. Wu, Z. Zhang, B. Zhao, H. Ma, W. Dang, Z. Wei, General synthesis of two-dimensional van der Waals heterostructure arrays, *Nature* 579 (7799) (2020) 368–374.
- [4] N. Li, Q. Wang, C. Shen, Z. Wei, H. Yu, J. Zhao, X. Lu, G. Wang, C. He, L. Xie, Large-scale flexible and transparent electronics based on monolayer molybdenum disulfide field-effect transistors, *Nat. Electron.* 3 (11) (2020) 711–717.
- [5] X. Chen, Y. Xie, Y. Sheng, H. Tang, Z. Wang, Y. Wang, F. Liao, J. Ma, X. Guo, Wafer-scale functional circuits based on two dimensional semiconductors with fabrication optimized by machine learning, *Nat. Commun.* 12 (1) (2021) 5953.
- [6] A.A. Balandin, Thermal properties of graphene and nanostructured carbon materials, *Nat. Mater.* 10 (8) (2011) 569–581.
- [7] E. Pop, Energy dissipation and transport in nanoscale devices, *Nano Res.* 3 (2010) 147–169.
- [8] A.L. Moore, L. Shi, Emerging challenges and materials for thermal management of electronics, *Mater. Today* 17 (4) (2014) 163–174.
- [9] Y. Wei, C. Deng, X. Zheng, Y. Chen, X. Zhang, W. Luo, Y. Zhang, G. Peng, J. Liu, H. Huang, Anisotropic in-plane thermal conductivity for multi-layer WTe₂, *Nano Res.* 15 (1) (2022) 401–407.
- [10] Y. Wei, R. Zhang, Y. Zhang, X. Zheng, W. Cai, Q. Ge, K.S. Novoselov, Z. Xu, T. Jiang, C. Deng, Thickness-independent energy dissipation in graphene electronics, *ACS Appl. Mater. Interfaces* 12 (15) (2020) 17706–17712.
- [11] A.A. Balandin, S. Ghosh, W. Bao, I. Calizo, D. Teweldebrhan, F. Miao, C.N. Lau, Superior thermal conductivity of single-layer graphene, *Nano Lett.* 8 (3) (2008) 902–907.
- [12] J.H. Seol, I. Jo, A.L. Moore, L. Lindsay, Z.H. Aitken, M.T. Pettes, X. Li, Z. Yao, R. Huang, D. Broido, Two-dimensional phonon transport in supported graphene, *Science* 328 (5975) (2010) 213–216.
- [13] Y. Fu, J. Hansson, Y. Liu, S. Chen, A. Zehri, M.K. Samani, N. Wang, Y. Ni, Y. Zhang, Z.-B. Zhang, Graphene related materials for thermal management, *2D Mater.* 7 (1) (2020), 012001.
- [14] Q. Cai, D. Scullion, W. Gan, A. Falin, S. Zhang, K. Watanabe, T. Taniguchi, Y. Chen, E.J. Santos, L.H. Li, High thermal conductivity of high-quality monolayer boron nitride and its thermal expansion, *Sci. Adv.* 5 (6) (2019) eaav0129.
- [15] Z.-Y. Ong, Y. Cai, G. Zhang, Y.-W. Zhang, Strong thermal transport anisotropy and strain modulation in single-layer phosphorene, *J. Phys. Chem. C* 118 (43) (2014) 25272–25277.
- [16] H. Song, J. Liu, B. Liu, J. Wu, H.-M. Cheng, F. Kang, Two-dimensional materials for thermal management applications, *Joule* 2 (3) (2018) 442–463.
- [17] S.E. Kim, F. Mujid, A. Rai, F. Eriksson, J. Suh, P. Poddar, A. Ray, C. Park, E. Fransson, Y. Zhong, Extremely anisotropic van der Waals thermal conductors, *Nature* 597 (7878) (2021) 660–665.
- [18] D. Chung, Y. Takizawa, Performance of isotropic and anisotropic heat spreaders, *J. Electron. Mater.* 41 (2012) 2580–2587.
- [19] N. Miao, B. Xu, L. Zhu, J. Zhou, Z. Sun, 2D intrinsic ferromagnets from van der waals antiferromagnets, *J. Am. Chem. Soc.* 140 (7) (2018) 2417–2420.
- [20] A. Nair, S. Rani, M.V. Kamalakar, S.J. Ray, Bi-stimuli assisted engineering and control of magnetic phase in monolayer CrOCl, *Phys. Chem. Chem. Phys.* 22 (22) (2020) 12806–12813.
- [21] X. Qing, H. Li, C. Zhong, P. Zhou, Z. Dong, J. Liu, Magnetism and spin exchange coupling in strained monolayer CrOCl, *Phys. Chem. Chem. Phys.* 22 (30) (2020) 17255–17262.
- [22] Y. Wang, X. Gao, K. Yang, P. Gu, X. Lu, S. Zhang, Y. Gao, N. Ren, B. Dong, Y. Jiang, Quantum Hall phase in graphene engineered by interfacial charge coupling, *Nat. Nanotechnol.* 17 (12) (2022) 1272–1279.
- [23] K. Yang, X. Gao, Y. Wang, T. Zhang, Y. Gao, X. Lu, S. Zhang, J. Liu, P. Gu, Z. Luo, Unconventional correlated insulator in CrOCl-interfaced Bernal bilayer graphene, *Nat. Commun.* 14 (1) (2023) 2136.
- [24] X. Zheng, Y. Wei, Z. Wei, W. Luo, X. Guo, X. Zhang, J. Liu, Y. Chen, G. Peng, W. Cai, Highly anisotropic thermal conductivity of few-layer CrOCl for efficient heat dissipation in graphene device, *Nano Res.* 15 (10) (2022) 9377–9385.
- [25] G. Kresse, J. Furthmüller, Efficiency of ab-initio total energy calculations for metals and semiconductors using a plane-wave basis set, *Comput. Mater. Sci.* 6 (1) (1996) 15–50.
- [26] J.P. Perdew, K. Burke, M. Ernzerhof, Generalized Gradient Approximation Made Simple, *Phys. Rev. Lett.* 77 (18) (1996) 3865–3868.
- [27] S. Grimme, J. Antony, S. Ehrlich, H. Krieg, A consistent and accurate ab initio parametrization of density functional dispersion correction (DFT-D) for the 94 elements H–Pu, *J. Chem. Phys.* 132 (15) (2010).
- [28] A. Togo, L. Chaput, T. Tadano, I. Tanaka, Implementation strategies in phonopy and phono3py, *J. Phys.: Condens. Matter* 35 (35) (2023), 353001.
- [29] A. Togo, First-principles phonon calculations with phonopy and Phono3py, *J. Phys. Soc. Jpn.* 92 (1) (2022), 012001.
- [30] W. Li, J. Carrete, N.A. Katcho, N. Mingo, ShengBTE: a solver of the Boltzmann transport equation for phonons, *Comput. Phys. Commun.* 185 (6) (2014) 1747–1758.
- [31] A.H. Castro Neto, F. Guinea, N.M.R. Peres, K.S. Novoselov, A.K. Geim, The electronic properties of graphene, *Rev. Mod. Phys.* 81 (1) (2009) 109–162.
- [32] H. Xie, M. Hu, H. Bao, Thermal conductivity of silicene from first-principles, *Appl. Phys. Lett.* 104 (13) (2014).
- [33] G. Qin, Q.-B. Yan, Z. Qin, S.-Y. Yue, M. Hu, G. Su, Anisotropic intrinsic lattice thermal conductivity of phosphorene from first principles, *Phys. Chem. Chem. Phys.* 17 (7) (2015) 4854–4858.
- [34] Q. Fan, J. Yang, H. Qi, L. Yu, G. Qin, Z. Sun, C. Shen, N. Wang, Anisotropic thermal and electrical transport properties induced high thermoelectric performance in an Ir₂Cl₂O₂ monolayer, *Phys. Chem. Chem. Phys.* 24 (18) (2022) 11268–11277.
- [35] J. Carrete, N. Mingo, S. Curtarolo, Low thermal conductivity and triaxial phononic anisotropy of SnSe, *Appl. Phys. Lett.* 105 (10) (2014).
- [36] L. Lindsay, Li Wu, Carrete Jesús, Mingo Natalio, A. D, Phonon thermal transport in strained and unstrained graphene from first principles, *Phys. Rev. B, Condens. Matter Mater. Phys.* 89 (15) (2014), 155426-1-155426-8.
- [37] L. Lindsay, D.A. Broido, N. Mingo, Flexural phonons and thermal transport in graphene, *Phys. Rev. B* 82 (11) (2010), 115427.
- [38] W. Li, J. Carrete, N. A. Katcho, N. Mingo, ShengBTE: a solver of the Boltzmann transport equation for phonons, *Comput. Phys. Commun.* 185 (6) (2014) 1747–1758.
- [39] X. Gu, Y. Wei, X. Yin, B. Li, R. Yang, Colloquium: phononic thermal properties of two-dimensional materials, *Rev. Mod. Phys.* 90 (4) (2018), 041002.
- [40] X. Li, K. Maute, M.L. Dunn, R. Yang, Strain effects on the thermal conductivity of nanostructures, *Phys. Rev. B* 81 (24) (2010), 245318.
- [41] H. Xie, T. Ouyang, É. Germaneau, G. Qin, M. Hu, H. Bao, Large tunability of lattice thermal conductivity of monolayer silicene via mechanical strain, *Phys. Rev. B* 93 (7) (2016), 075404.
- [42] H. Liu, G. Qin, Y. Lin, M. Hu, Disparate strain dependent thermal conductivity of two-dimensional penta-structures, *Nano Lett.* 16 (6) (2016) 3831–3842.
- [43] C. Zhang, J. Sun, Y. Shen, W. Kang, Q. Wang, Effect of high order phonon scattering on the thermal conductivity and its response to strain of a Penta-NiN₂ sheet, *J. Phys. Chem. Lett.* 13 (25) (2022) 5734–5741.